Atomic structure of SiO_2 glass and its response to pressure

Lars Stixrude and M. S. T. Bukowinski
Department of Geology and Geophysics, University of California at Berkeley, Berkeley, California 94720
(Received 29 October 1990; revised manuscript received 14 February 1991)

We describe the results of Monte Carlo simulations of SiO_2 glass based on a covalent-potential model of tetrahedral Si-O bonding. The potential model has been shown to accurately reproduce the structure, compression mechanisms, and phase stability of the corresponding crystalline and liquid phases. The simulations are in good agreement with the measured equation of state of silica glass. We compare the simulated structure with experimental data directly by performing "experiments" on the simulated glass—determining the expected diffraction pattern based on our simulated structure—and find good agreement with the observed structure. We show that, unlike the case in SiO_2 crystals, changes in the local structure of glass are insufficient to account for its compression. Measures of the medium-range structure, including cluster population and geometry and ring statistics, vary significantly with pressure and indicate a significant topological component to the compression of glass. We use a simple model for the effects of ring formation on density to analyze the topological changes and show that characteristic ring size increases with increasing compression, consistent with the increase in ring size with increasing density found previously in tectosilicate crystals and in simulations of SiO_2 liquid. We discuss prospects for experimental verification of the predicted pressure-induced structural changes.

I. INTRODUCTION

The last decade has seen considerable debate over the atomic structure of SiO_2 glass.[1,2] Recently, however, precise neutron diffraction experiments[3] and structural models, including one which agrees quantitatively with diffraction data,[4] have apparently confirmed that SiO_2 glass consists of a nearly perfect network of corner-sharing SiO_4 tetrahedra, a structure proposed by Zachariasen[5] in 1932. Despite their success, Zachariasen's theory and its modern counterpart, the continuous random network (CRN) theory,[6] remain incomplete. Although the CRN provides a detailed description of the distribution of nearest-neighbor-bond distances and angles, it still falls short of being able to specify a model of the atomic structure of glass. This is effectively illustrated by past modeling efforts which have adopted a wide variety of protocols and assumptions in addition to CRN precepts in order to construct tangible continuous random networks. Among these are hand-built ball-and-stick models,[7] their computer-generated analogs,[8] and bond-switching algorithms.[9] These modeling efforts have uniformly revealed a remarkably rich and complex structure, whose meaningful description, beyond the prescriptions of the CRN theory, presents a considerable challenge.

Missing from the CRN theory is a detailed description of the glass structure on length scales larger than the basic bitetrahedral unit. The large class of tectosilicate structures, of which SiO_2 glass is a member, shows the importance of variations in this medium-range structure in characterizing continuous tetrahedral networks.[10] All tectosilicate structures are based on a continuous framework of corner-sharing TO_4 tetrahedra (where T is Si or Al). Despite large differences in composition and twofold variation in framework density ρ_F, the number of T atoms per unit volume), local geometries among the amorphous and the more than 80 topologically distinct crystalline tectosilicates are nearly invariant: T-O, O-O, and T-T distances vary by no more than 10%. Medium-range structure, however, is highly variable and measures of its geometry and topology (such as ring statistics) rationalize the wide range of observed densities.[10]

Although little is known experimentally about the response of glass structure to pressure, variations in medium-range structure may play a central role in the compression of amorphous SiO_2. Simulations indicate that nearly twofold compression of SiO_2 liquid induces large changes in medium-range structure but almost no changes in nearest-neighbor distances.[11] Here we analyze the structure of SiO_2 glass and propose that although local structure is also significantly affected, medium-range structure changes substantially with pressure and contributes significantly to its compression.

We combine Monte Carlo simulations with a simple but accurate model of covalent Si—O bonding to investigate the structure and compression mechanisms of SiO_2 glass. We first describe the potential model and then the simulations, paying particular attention to their convergence characteristics. We show that the simulated glass is in excellent agreement with the measured zero-pressure structure of glass and the experimental equation of state. We describe pressure-induced changes in glass structure and show that changes in local structure alone are insufficient to account for compression. We introduce measures of the medium-range structure, including ring and cluster statistics and cluster geometry, and show how these help explain the structure and compression in SiO_2 glass.

 ©1991 The American Physical Society

II. THE POTENTIAL MODEL

We have designed[12] a simple covalent potential model of bonding in four-fold coordinated phases of SiO_2. The model successfully reproduces the structure and equations of state of fourfold-coordinated SiO_2 crystals and the structure and compressibility of SiO_2 liquid.[12,13] The potential energy is given by

$$U=\sum_{i=1}^{N_{Si}}\sum_{j=1}^{4} f_c(r_{ij})D[\exp[2\beta(r_{ij}-r_0)]-2\exp[\beta(r_{ij}-r_0)]]$$
$$+\sum_{i=1}^{N_{Si}}\sum_{j=1}^{4}\sum_{i>j}^{4} f_c(\max\{r_{ij},r_{ik}\})g_\alpha(\alpha_{ijk}-\alpha_0)^2+\sum_{i=1}^{N_O}\sum_{j=1}^{2}\sum_{k>j}^{2} f_c(\max\{r_{ij},r_{ik}\})g_L(r_{jk}-L_0)^2+\sum_{i=1}^{N_O}\sum_{j>i}^{N_O} A\exp\left[-\frac{r_{ij}}{b}\right] \quad (1)$$

and

$$f_c(r_{ij})=\frac{1}{1+\exp[\gamma(r_{ij}-r_c)]}\ , \quad (2)$$

where N_{Si} and N_o are the number of Si and O atoms, respectively, r_{ij} is the distance between atoms i and j, and α_{ijk} is the intratetrahedral O—Si—O angle. The values of all parameters are given in Table I.

The multiple summations in the first three terms include only the four nearest O atoms about a Si atom and the two nearest Si atoms about an O atom. While the application of this tetrahedral nearest-neighbor condition is straightforward in crystalline structures, the more irregular structures encountered in simulations of liquids and glasses require two supplementary conditions. Thus, we require that among a Si atoms's four nearest O neighbors, it is bonded only to those which are not closer to two other Si atoms and, similarly, that among an O atoms's two nearest Si neighbors, it is bonded only to those which are not closer to four other O atoms. With these conditions, the potential energy [Eqs. (1) and (2)] is unambiguously defined for any arrangement of Si and O atoms. Although no more than four Si—O bonds per Si atom, and two per O atom are allowed, coordination numbers are not otherwise restricted and a tetrahedral structure is not imposed on the simulated glass. Further, there are no restrictions against bonds breaking and reforming and, in fact, we show below that bond rearrangement is an important compression mechanism in silica glass.

TABLE I. Parameters of the interatomic force model [Eqs. (1) and (2)]. Note: the energy unit, $E_0=10^{-19}$ J.

Parameter	Value
D	$7.33E_0$
β	2.0 Å^{-1}
r_0	1.604 29 Å
g_α	$3.89E_0$ rad^{-2}
α_0	109.47°
g_L	$4.38E_0$ Å^{-2}
L_0	3.0325 Å
A	7.5×10^6E_0
b	0.14 Å
r_c	2.5 Å
γ	20 Å^{-1}

We intend this model to describe only the bonding in structures with fourfold Si—O coordination. This is manifested not only in the limited number of bonds per Si, but also in the form and parametrization of the potential, which must differ substantially from that necessary to describe bonding in sixfold-coordinated structures. Because it disallows coordinations higher than four, the model can represent glass structure only up to the pressure of the four- to sixfold-coordination change, which is thought to be above 20 GPa (Ref. 14). We expect the model to be accurate to at least this pressure and to provide a realistic picture of glass structure and compression throughout the fourfold-coordinated pressure regime.

Several other potential models, based on the assumption that bonding in SiO_2 is ionic, have been used to study the fourfold to sixfold-coordination changes in amorphous silica.[15–18] While these simulations provide useful insight into the nature of pressure-induced coordination changes in ionic liquids in general, it is difficult to relate the results to SiO_2 in particular. For most ionic models, agreement with the compression of SiO_2 crystals is poor and the equation of state of SiO_2 glass has not previously been reproduced accurately over any pressure range.[18,19] Because *ab initio* calculations suggest that even the octahedral Si—O bond is not ionic,[20] it seems likely that a complete empirical model must include covalency and an explicit description of how bonding changes with coordination. It is hoped that our model will provide a well-characterized base line and a starting point for the construction of such a generalized model.

III. MONTE CARLO SIMULATIONS

A. Procedure

The simulations were performed in the constant particle number, pressure, and temperature (N-P-T) ensemble. The model glass consists of 192 atoms repeated with the usual periodic boundary conditions to minimize finite-size effects. Although larger systems were not tested, the primary cell was large enough (15 Å on a side at zero pressure) so that the radial distribution function fluctuated less than 2% about its long-range limiting value (unity) at half the cell size. The maximum allowable volume fluctuation and atomic displacement were chosen so that approximately 50% of new configurations were accepted. The volume was allowed to change with each new

configuration. The convergence characteristics of the simulations were analyzed in detail (see below) and run lengths of 4–12 million configurations were found adequate to achieve stability. We make the standard assumption that quantum effects are negligible, supported in our case by the very small de Broglie thermal wavelength compared with average interatomic separations.[21,22]

The entire course of the simulations described here is summarized by a volume-configuration number diagram (Fig. 1). The simulated glass was formed by using the final configuration of the fully equilibrated 2000 K, zero pressure liquid simulation (described in detail in Ref. 13) to initialize the glass simulation at 300 K and zero pressure. Simulations at each pressure consist of a stabilization period of 4–12 million configurations followed by an additional 4 million configurations for collecting average physical properties. The resulting average values of volume, $\langle V \rangle$, are shown in Table II. Their uncertainties, δ, were estimated by the blocking method.[23]

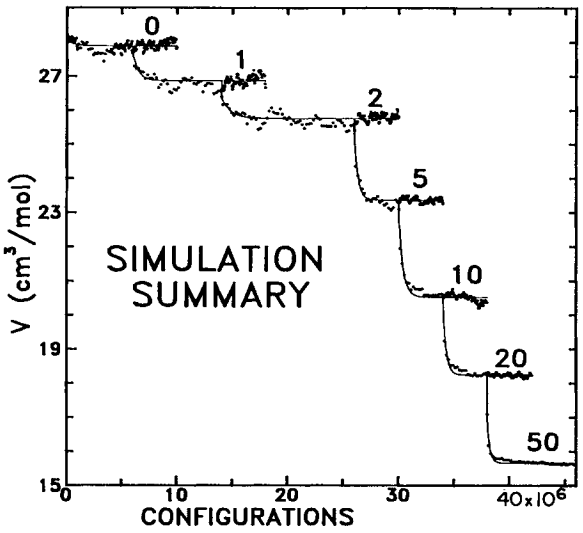

FIG. 1. Summary of the Monte Carlo simulations showing the progress of the molar volume. Each branch summarizes the simulations at one pressure which consists of a stabilization period, during which volume convergence is achieved, and an averaging period. The pressure is incremented at the end of the stabilization period resulting in a rapid decrease in volume. Each dot represents a mean volume averaged over 200 000 configurations for the stabilization period and 50 000 configurations for the averaging period. The lines are exponential fits (3) to the simulations records which are used to analyze the convergence of the simulations (see text and Table II).

B. Convergence

Estimation of converged values and their uncertainties is contingent on one's ability to identify the length of the initial transient. Identification of the transient is also of central practical importance since it determines the required length of a simulation and thus the requisite amount of computer time. Despite its importance, no generally acceptable method for identifying initial transients exists and it is usually done in a subjective manner (by eye).[24] While inspection of Fig. 1 certainly suggests that the simulations attain convergence during the stabilization period at each pressure, more objective assessments of convergence are possible.

We have found the convergent trend in our simulations to be systematic and easily identified. All the records approximate an exponential decay:

$$V'(t)=V'_\infty+(V_0-V'_\infty)\exp\left[-\frac{(t-t_0)}{\tau}\right], \qquad (3)$$

where the prime distinguishes the fit from the actual simulation record $V(t)$ (t is the configuration number and t_0 is its initial value), V_0 is the initial volume and the limiting value of V', V'_∞, and the "time" constant, τ are determined by a least-squares fit to $V(t)$ (see Table II and Fig. 1). The convergent trend is easily identified in part because the overall change in volume is always much larger than statistical fluctuations about the trend: the standard deviation of the fit σ does not exceed 1% of $\langle V \rangle$, and in most cases is an order of magnitude smaller than the difference between V'_∞ and V_0. The fits confirm that the simulations converge rapidly: τ is typically 4% of the total simulation length and V'_∞ is indistinguishable from our estimates of average stable values $\langle V \rangle$ (they differ by less than 2δ), for all pressures. We estimate the length of the initial transient T by the value of t after which $V'(t)$ no longer changes significantly, that is, when

TABLE II. Monte Carlo volumes. Units of P are GPa. Units of $\langle V \rangle$, V'_∞ and σ are cm^3/mol. Units of τ and T are millions of configurations. For $\langle V \rangle$, the uncertainty in the last digits reported (δ) is given in parentheses.

P	$\langle V \rangle$	V'_∞	τ	σ	T
0	27.933(29)	27.887	0.373	0.134	1.1
1	26.889(45)	26.863	0.479	0.160	1.5
2	25.790(31)	25.757	0.816	0.140	2.5
5	23.362(44)	23.358	0.326	0.100	1.3
10	20.507(58)	20.519	0.393	0.132	1.5
20	18.232(9)	18.241	0.291	0.089	1.7
50	15.641(17)	15.652	0.249	0.060	1.1

$V'(t)$ equals $V'_\infty + \delta$. For all pressures, T is much smaller than the total simulation length and always well within the stabilization period (Table II). Thus, it appears that the simulations are well converged, and, hence, that average properties at higher pressures are unbiased by transients.

IV. COMPARISON WITH EXPERIMENTAL DATA

A. Equation of state

The equation of state of the simulated glass is shown in Table II. The zero pressure volume of glass is overestimated by only 2% and the overall agreement with the experimental equation of state is very good up to 10 GPa (Fig. 2), the approximate upper limit of hydrostaticity in these experiments.[25] The average deviation between experimental and simulated volumes over this pressure interval is similar to experimental uncertainties (1%). The reason for the discrepancy between the highest pressure data of Bridgman[26] with both our simulations and the later experiments is not clear but may be due to inaccurate pressure calibration in Bridgman's experiments.[25] Because the model also reproduces the equations of state of tetrahedral SiO_2 crystals to at least 20 GPa, we expect

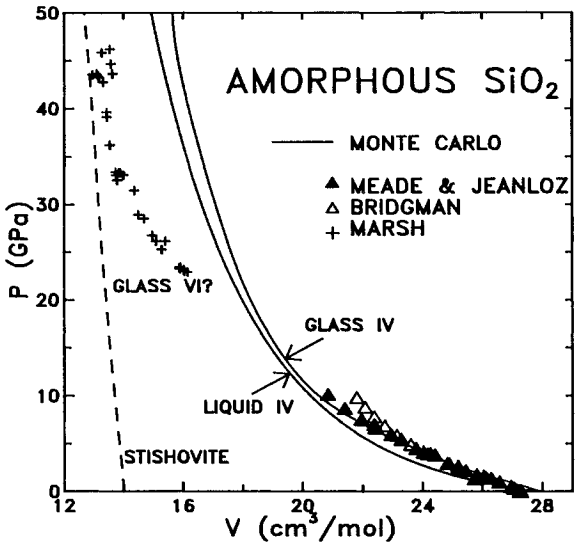

FIG. 2. Pressure-volume relations of SiO_2 glass and liquid from our Monte Carlo simulations (solid lines) compared with experimental data (symbols). The line farthest to the right represents Monte Carlo simulation results for SiO_2 glass. The neighboring line represents Monte Carlo simulation results for SiO_2 liquid at 2000 K (Ref. 13). The larger volume of the simulated glass compared with the liquid is the result of kinetic hindrances to pressure-induced structural change in the glass. The triangles and circles are the results of static pressure experiments (Refs. and 25 and 26) up to the approximate limit of hydrostatic pressure in the latter experiments. The crosses are the results of shock wave experiments on silica glass (Ref. 27). The fact that the shocked glass is much denser than the simulated fourfold-coordinated glass suggests that the experimental glass contains significant amounts of octahedrally coordinated Si.

the simulations to provide an accurate picture of compression over the entire pressure range of fourfold coordination in the glass.

The simulated glass remains fourfold coordinated at high pressure since the model disallows higher coordinations. The greater experimental densities[27] above 20 GPa are almost certainly caused by the presence of sixfold Si-O coordination in the shocked glass, due either to the formation of stishovite or to a gradual pressure-induced coordination increase. Octahedral coordination in the high pressure glass is also suggested by the similarity of the densities of shocked glass and octahedrally coordinated stishovite[28] above 40 GPa (Fig. 2). The slightly lower density of shocked glass compared with stishovite may be due to the high shock temperature.

B. Radial structure

The *radial distribution function* $g(r)$ in a multicomponent system is defined by

$$n_{\alpha\beta}(R)=\rho c_\beta \int_0^R g_{\alpha\beta}(r)d\mathbf{r} , \tag{4}$$

where c_γ is the concentration of atom γ (number of atoms of type γ divided by the total number of atoms), ρ is the number density, and $n_{\alpha\beta}(R)$ is the number of β atoms within a distance R of an α atom. The total radial distribution function is

$$g(r)=\sum_\alpha \sum_\beta c_\alpha c_\beta g_{\alpha\beta}(r) , \tag{5}$$

where the sums are over the different atom types. Figure 3 shows the $g_{\alpha\beta}(r)$ for the simulated glass. The experimentally determined quantity $H'(k)$ is related to a convolution of $g(r)$ with the atomic form factors

$$H'(k)=\sum_\alpha \sum_\beta c_\alpha c_\beta F'_{\alpha\beta}(k)h'_{\alpha\beta}(k) , \tag{6}$$

where $h'_{\alpha\beta}(k)$ is the nondimensional Fourier transform of $h_{\alpha\beta}(r)=g_{\alpha\beta}(r)-1$:

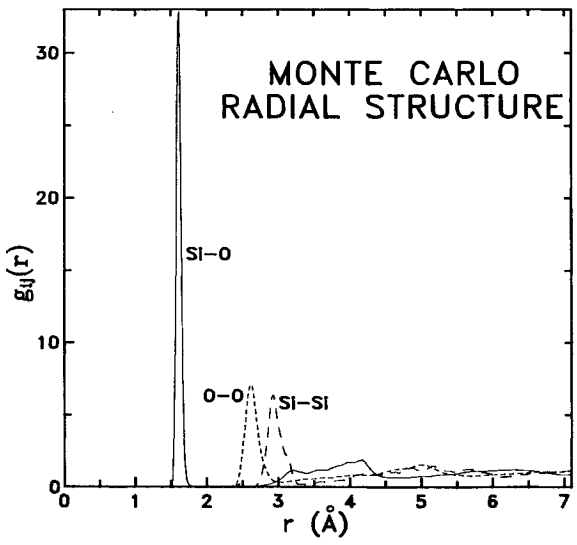

FIG. 3. Component radial distribution functions $g_{\alpha\beta}(r)$ (4) at zero pressure from the Monte Carlo simulations.

$$h'_{\alpha\beta}(k)=\rho\int h_{\alpha\beta}(r)e^{i\mathbf{k}\cdot\mathbf{r}}d\mathbf{r} \tag{7}$$

and $F'_{\alpha\beta}(k)$ contains the atomic form factors $f_\gamma(k)$, which, in general, depend on k, the type of atom, and the type of radiation (neutrons, electrons, or x rays):

$$F'_{\alpha\beta}(k)=\frac{f_\alpha(k)f_\beta(k)}{\left[\sum_\gamma c_\gamma f_\gamma(k)\right]^2} . \tag{8}$$

The Fourier transform of $H'(k)$ is

$$H(r)=\frac{1}{\rho(2\pi)^3}\int H'(k)e^{-i\mathbf{k}\cdot\mathbf{r}}d\mathbf{k} . \tag{9}$$

To compare our simulations directly with data we perform diffraction "experiments" in which we calculate the $H'(k)$ that an experiment on our simulated glass would measure. We calculate $H'(k)$ from (6) by transforming the $h_{\alpha\beta}(r)$ determined in our simulations and combining them with the x-ray and neutron atomic form factors $f_\gamma(k)$ from standard references.[29,30] The diffraction patterns are compared with experimental data in Figs. 4 and 5. For $k>2$ Å^{-1}, the agreement is good. For both neutron and x-ray diffraction the differences between simulation and data are comparable to the differences between different experiments and in the case of x rays must be due in part to our use of free-atom scattering factors, which are universally adopted but probably unrealistic in detail for a covalently bonded material such as silica. The position of the peak at small k is reproduced but its amplitude is underestimated by the simulations. While an inaccurate simulated structure cannot be completely ruled out, the finite range in r used to calculate the simulated diffraction patterns will lower the peak height (see also Ref. 31) and this alone may account for the disagreement. The model's ability to reproduce the remaining structural features, as well as the zero pressure density and the equation of state, also suggests that this single exception may be an artifact. Moreover, the simulations

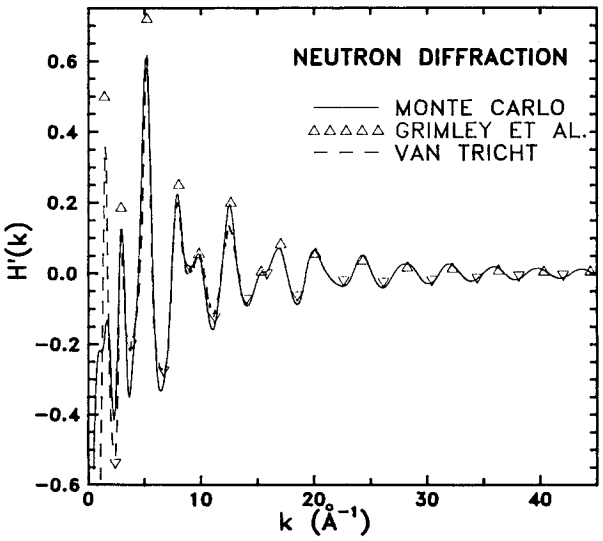

FIG. 4. Comparison between neutron diffraction data (Refs. 3 and 45) and the predictions of the Monte Carlo simulations.

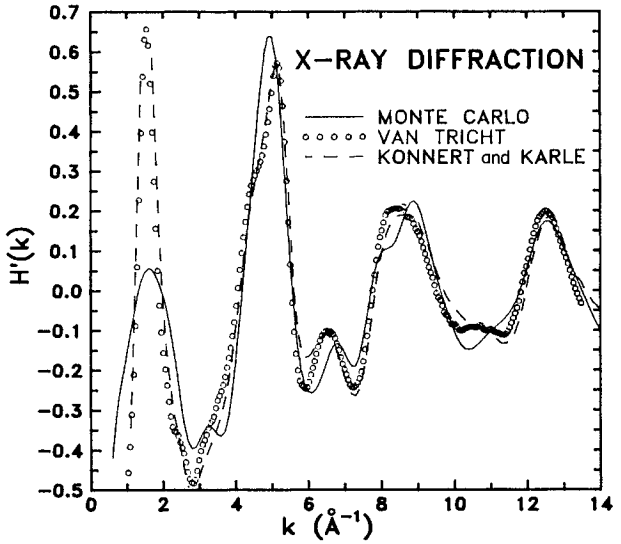

FIG. 5. Comparison between x-ray diffraction data (Refs. 43 and 45) and the predictions of the Monte Carlo simulations.

appear to match the data as well as many other empirical structural models which were specifically optimized to minimize disagreement with the observed structure.[8,31–34]

In real space, the shape of the experimental $H(r)$ is affected not only by the $f_\gamma(k)$ but also by the finite range in k over which $H'(k)$ is measured. Because sudden truncation at a finite k_{max} leads to unphysical oscillations in $H(r)$, a filter is often applied to the data by multiplying the observed $H'(k)$ by a modification function, $M'(k)$, which goes smoothly to zero at large k. To compare our simulations directly with experiment we calculate $H(r)$ from (9), truncating the Monte Carlo $H'(k)$ at the appropriate experimental k_{max} and applying the same filters that were used in the experimental data analysis (Figs. 6

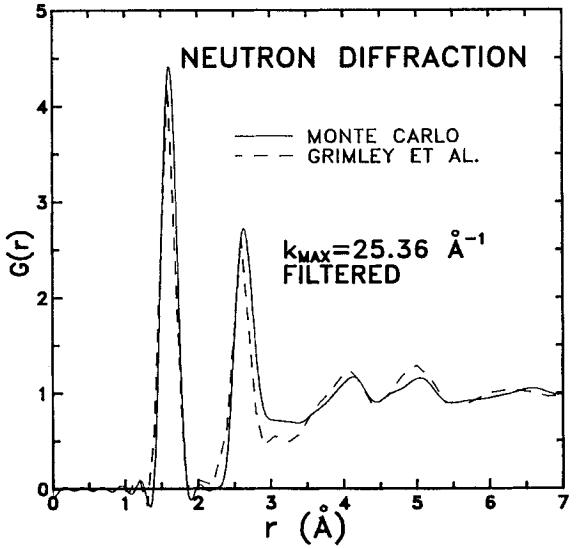

FIG. 6. $G(r)$ calculated from the Monte Carlo simulations (solid line) from (9) with a filter: $M'(k)=\sin(\pi k/k_{max})/(\pi k/k_{max})$, and $k_{max}=25.36$ Å^{-1}, compared with the $G(r)$ calculated in the same way from the data of Ref. 3.

and 7). The overall agreement between experiment and simulation is very good and is comparable to the agreement in reciprocal space. The positions and heights of the first five peaks (corresponding to Si-O, O-O, Si-Si, 2nd, Si-O, and 2nd O-O, and 2nd Si-Si correlations) are well matched by the simulations except the first Si-Si peak which is somewhat too high and occurs at a distance 0.1 Å smaller than experiment.

Although the experimental $G(r)$ cannot be rigorously separated into its component distributions, component nearest-neighbor distances $r_{\alpha\beta}$, standard deviations $\sigma_{\alpha\beta}$, and nearest-neighbor coordination numbers $n_{\alpha\beta}$, can be extracted by an approximate modeling procedure. These approximate structural measures do not depend critically on the details of the modeling or experimental parameters (e.g., $k_{\max}$ or the type of radiation) and thus serve as a useful additional test of our simulations. We calculated $r_{\alpha\beta}$, $\sigma_{\alpha\beta}$, and $n_{\alpha\beta}$ from the simulations by averaging over all bonded Si-O pairs and all linked O-O and Si-Si pairs (pairs which are bonded to a common Si or O, respectively) in five different configurations, spaced one million configuration apart.

Table III compares the structural parameters determined from neutron and x-ray diffraction experiments with the Monte Carlo values. The simulated Si-O and O-O distances are approximately 1% larger than experimental values while the simulated Si-Si distance is approximately 3% too small. The simulations predict a somewhat sharper Si-O distribution than is observed and a smaller Si-Si coordination number, although the latter is probably the parameter least well constrained by experiment. All the other predicted parameters fall within the experimental range and, overall, the agreement is very good.

Although the agreement of the simulations with the observed properties of SiO_2 glass is generally excellent, the discrepancy in the position of the first $g_{\text{Si-Si}}$ peak may indicate the need for a more complex functional form of the Si-Si potential, or a model which includes Coulombic forces, such as the CM.[12] Nevertheless, the overall level of agreement with experimental structure and compression is remarkable, especially considering that no glass data were used to constrain our interatomic force model.

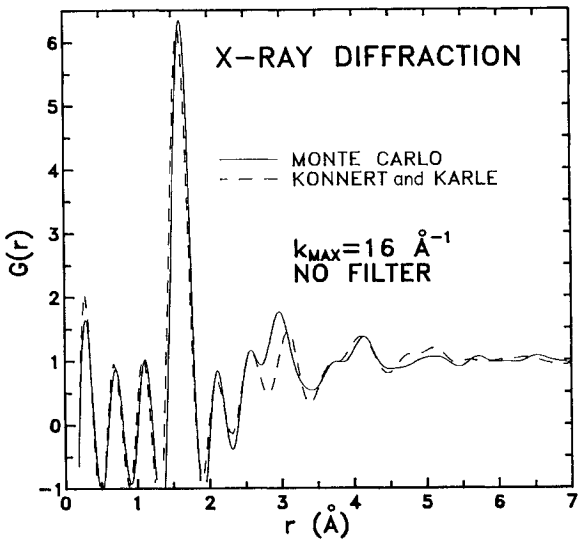

FIG. 7. $G(r)=H(r)+1$ calculated from the Monte Carlo simulations (solid line) from (9) with $k_{\max}=16$ Å^{-1}, compared with the $G(r)$ calculated in the same way from the data of Ref. 43.

V. STRUCTURE AND COMPRESSION

A. Local structure at $P=0$

Although the model does not impose fourfold coordination, the simulations produce a glass structure which is a nearly perfect continuous random network of corner-sharing SiO_4 tetrahedra. The predicted coordination numbers are nearly ideal ($n_{\text{Si-O}}=4$, $n_{\text{O-O}}=6$, $n_{\text{Si-Si}}=4$); the slightly smaller values indicate the presence of some three coordinated Si atoms and one coordinated (nonbridging) O atoms (12%) (Table III). Diffraction data, which provide the best experimental measures of coordination number, also indicate slightly lower than ideal values (Table III). Despite the presence of some nonideal coordination environments, perfect coordination, a precept of the modern CRN theory (although not of Zachariasen's original model) is clearly a very good approximation and a useful idealization. Further, the ratio

TABLE III. Structural parameters.

	P (GPa)	$r_{\text{Si-O}}$	$\sigma_{\text{Si-O}}$	$n_{\text{Si-O}}$	$r_{\text{O-O}}$	$\sigma_{\text{O-O}}$	$n_{\text{O-O}}$	$r_{\text{Si-Si}}$	$\sigma_{\text{Si-Si}}$	$n_{\text{Si-Si}}$
Experiment ($P=0$)	Ref. 3	1.608	0.047	3.85	2.626	0.091	5.94	3.077	0.111	4.00
	Ref. 43	1.595	0.051	4.00	2.629	0.099	5.94	3.077	0.111	4.13
	Ref. 44[a]	1.62	0.087	3.9	2.65	0.102	5.5	3.11	0.141	3.9
	Ref. 44[b]	1.62	0.078	4.1	2.66	0.095	6.2	3.10	0.132	4.4
Simulations	0	1.634	0.032	3.875	2.666	0.093	5.609	2.996	0.116	3.719
	1	1.634	0.032	3.875	2.666	0.092	5.609	2.988	0.118	3.719
	2	1.630	0.031	3.875	2.659	0.092	5.609	2.973	0.118	3.719
	5	1.631	0.044	3.878	2.658	0.106	5.619	2.944	0.132	3.725
	10	1.629	0.050	3.897	2.651	0.128	5.675	2.908	0.149	3.763
	20	1.621	0.040	3.894	2.632	0.135	5.666	2.859	0.155	3.756
	50	1.607	0.038	3.906	2.599	0.174	5.703	2.798	0.180	3.781

[a]X-ray-diffraction data.
[b]Neutron-diffraction data.

of $r_{O\text{-}O}$ to $r_{Si\text{-}O}$ has almost the value expected for ideal SiO_4 tetrahedra, $(\frac{8}{3})^{1/2}$ and the intertetrahedral distances ($r_{Si\text{-}Si}$) are both longer and more variable (larger $\sigma_{\alpha\beta}$) than tetrahedral ones, consistent with the continuous random network model.

Angle distributions $B_{\alpha\beta\gamma}(\theta)$ (Table IV and Fig. 8) can also be understood in terms of a continuous random network. These distributions, like the calculations of $r_{\alpha\beta}$, $\sigma_{\alpha\beta}$, and $n_{\alpha\beta}$, involve only bonded and linked pairs and are compiled using five configurations spaced one million configurations apart. The dominant peaks in the angular distribution functions, $B_{\alpha\beta\gamma}(\theta)$, for which at least two of the subscripts refer to O atoms, are due to tetrahedral geometry. The O-Si-O distribution is peaked very near the ideal tetrahedral angle, $\cos^{-1}(-\frac{1}{3})=109.47°$, the peak near 60° in the O-O-O distribution arises from the equilateral triangles which form the faces of ideal tetrahedra, and the O-O-Si distribution is peaked near $\frac{1}{2}(180-109.47)=35.26°$. The O-O-Si and O-O-O- distributions are bimodal, with broad features due to intertetrahedral geometries in addition to the sharp intratetrahedral peaks.

Angular distributions for which at least two atoms are Si are much broader, largely because intertetrahedral forces are much weaker than intratetrahedral forces. The Si-O-Si distribution is broad and asymmetric with an average value of $\theta_{Si\text{-}O\text{-}Si}=135°$, approximately 5% smaller than estimates from diffraction[35] and NMR data,[36] due to the small Monte Carlo value of $r_{Si\text{-}Si}$ noted above. The Si-Si-O distribution has one peak at small angles near $\frac{1}{2}(180-\theta_{Si\text{-}O\text{-}Si})=23.5°$ due to Si-O-Si bridges, and a broader feature corresponding to angles in which the O atom does not bridge the two Si atoms. The Si-Si-Si distribution has two peaks, a broad one centered near the ideal tetrahedral angle (109.47°) and a sharp one centered

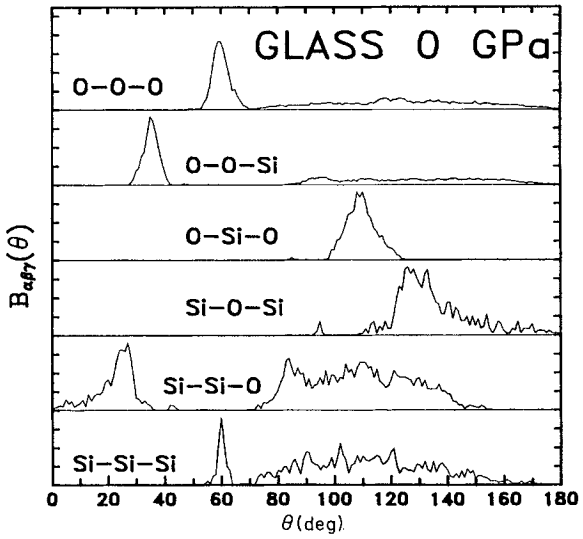

FIG. 8. Angle distributions $B_{\alpha\beta\gamma}(\theta)$ from the Monte Carlo simulations at zero pressure. All distributions are scaled to the same (arbitrary) maximum height.

TABLE IV. Angle Distributions, $B_{\alpha\beta\gamma}(\theta)$. The first and second columns for each distribution are $\theta_{\alpha\beta\gamma}$ and $\sigma_{\alpha\beta\gamma}$, respectively. The distributions (Si-Si-O, O-O-Si, O-O-O) which are clearly bimodal at all pressures have been subdivided into two subdistributions, each with its own average and standard deviation. Units of P are GPa.

P	$\theta_{Si\text{-}Si\text{-}Si}$	$\sigma_{Si\text{-}Si\text{-}Si}$	$\theta_{Si\text{-}Si\text{-}O}$	$\sigma_{Si\text{-}Si\text{-}O}$	$\theta_{Si\text{-}O\text{-}Si}$	$\sigma_{Si\text{-}O\text{-}Si}$	$\theta_{O\text{-}Si\text{-}O}$	$\sigma_{O\text{-}Si\text{-}O}$	$\theta_{O\text{-}O\text{-}Si}$	$\sigma_{O\text{-}O\text{-}Si}$	$\theta_{O\text{-}O\text{-}O}$	$\sigma_{O\text{-}O\text{-}O}$
0	106.6	26.8	22.6	7.2	108.4	18.3	134.8	14.4	109.5	5.5	35.3	2.8	126.9	24.0	60.1	3.1	123.8	25.1
1	106.2	26.8	22.9	7.4	108.3	18.3	134.2	14.8	109.4	5.3	35.3	2.7	126.3	24.0	60.1	3.1	123.5	25.2
2	106.0	26.9	23.4	6.9	108.2	18.5	133.1	13.9	109.4	5.3	35.3	2.7	125.8	24.1	60.2	3.1	123.3	25.3
5	105.3	27.3	24.7	7.1	107.9	19.5	130.6	14.1	109.3	5.7	35.3	2.9	123.6	24.4	60.1	3.3	122.3	25.4
10	104.8	28.1	26.0	7.3	107.6	21.2	128.0	14.5	109.1	7.1	35.4	3.6	121.3	25.0	60.0	3.9	121.0	25.8
20	103.9	28.6	27.2	7.9	107.2	22.4	125.6	15.7	108.9	7.9	35.5	4.0	119.0	25.4	59.9	4.2	120.5	25.6
50	102.8	29.1	28.4	8.6	106.5	23.9	123.3	17.2	108.5	10.4	35.8	5.3	116.9	26.3	59.3	5.0	118.6	26.1

at 60° which corresponds to three-membered rings. This bimodal distribution has also been found in reverse Monte Carlo simulations,[4] indicating that real glass, like our simulated one, contains a significant number of three-membered rings (ring statistics are discussed further below). All the angular distributions agree very well with those found with the reverse Monte Carlo technique.

B. Local structure at pressure

Despite the nearly twofold variation in volume considered here, intratetrahedral geometries do not change substantially. In particular, $r_{\text{Si-O}}$ and $r_{\text{O-O}}$ decrease by less than 2 and 3 %, respectively, over 50 GPa (Table III and Fig. 9). Further, the intratetrahedral angle distributions $B_{\text{O-Si-O}}$ and the small angle components of $B_{\text{O-O-O}}$ and $B_{\text{O-O-Si}}$, change their average values by less than a degree (Table IV). Thus, although pressure-induced increases in the corresponding $\sigma_{\alpha\beta}$ and $\sigma_{\alpha\beta\gamma}$ indicate that intratetrahedral geometries distort somewhat with compression, the glass remains a tetrahedral network up to the highest pressure considered here.

The weaker intertetrahedral forces allow the corresponding geometrical parameters to deform more with pressure. Thus, the pressure-induced decrease in $r_{\text{Si-Si}}$ is more than twice that of $r_{\text{Si-O}}$ and $r_{\text{O-O}}$ (Table III and Fig. 9). Further, the intertetrahedral angle distributions, including $B_{\text{Si-Si-Si}}$, $B_{\text{Si-O-Si}}$, $B_{\text{Si-Si-O}}$, and the large angle components of $B_{\text{O-O-Si}}$ and $B_{\text{O-O-O}}$, are affected strongly by pressure (Table IV). The approximately 11-degree decreases in $\theta_{\text{O-O-Si}}$ and $\theta_{\text{Si-O-Si}}$ and the complementary 5.5-degree increase in the small angle component of $\theta_{\text{Si-Si-O}}$ are a direct result of the decrease in $r_{\text{Si-Si}}$. $\theta_{\text{O-O-O}}$ and $\theta_{\text{Si-Si-O}}$, which are also affected by torsion about the bridging oxygen, show somewhat smaller changes with pressure. $\theta_{\text{Si-Si-Si}}$ also decreases and all the distributions grow broader with pressure, indicating distortion of the tetrahedral framework.

Although intertetrahedral geometries vary significantly with pressure, the changes are less than expected by analogy with crystalline phases.[13] The compression of SiO_2 crystals can be explained almost entirely by decreases in $\theta_{\text{Si-O-Si}}$ or, equivalently, in $r_{\text{Si-Si}}$. Specifically, crystalline volumes scale with $r_{\text{Si-Si}}$ so that the nondimensional quantity $(r^3_{\text{Si-Si}}/V)$ is approximately independent of pressure (Fig. 10). In the glass however, $r_{\text{Si-Si}}$ changes more slowly than $V^{1/3}$, causing the ratio to increase 20% over the pressure range considered here (Figs. 9 and 10). Although there are no measurements of glass structure at pressure, our results are consistent with a zero pressure x-ray diffraction experiment on an irreversibly compacted sample which shows that a 16% densification leads to only a 2% change in $r_{\text{Si-Si}}$ (Ref. 37). Thus, decreases in intertetrahedral distance cannot completely account for the compression of SiO_2 glass and an additional compression mechanism must be operating. We have observed similarly unusual compressional behavior, although even more pronounced, in Monte Carlo simulations of SiO_2 liquid.[11] The liquid compresses without substantial changes in $r_{\text{Si-Si}}$ by rearranging the bonding topology of

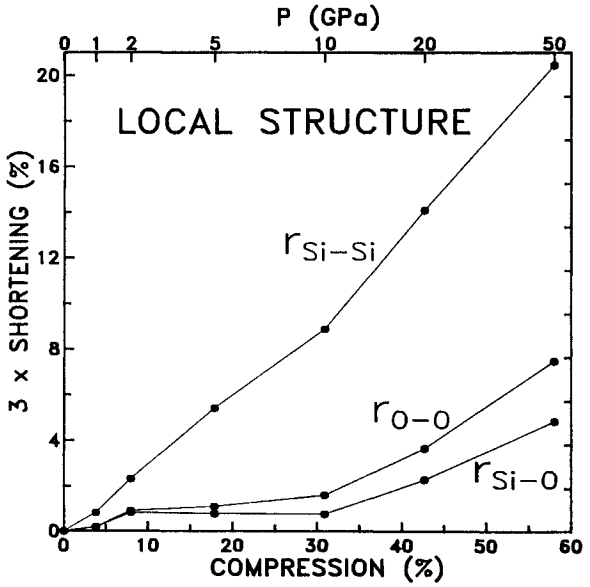

FIG. 9. Pressure induced shortening of $r_{\alpha\beta}$ $(-300\ln[r_{\alpha\beta}(P)/r_{\alpha\beta}(0)])$ vs percent volume change $(-100\ln[V(P)/V(0)])$. The corresponding pressure is indicated on the upper horizontal axis. The change in $r_{\alpha\beta}$ is multiplied by a factor of 3 to permit comparison with the change in volume. The pressure interval where the $r_{\alpha\beta}$ change the least, 2–10 GPa ($r_{\text{Si-O}}$ actually increases slightly over this interval), coincides with the interval of greatest topological change in the glass (Fig. 11).

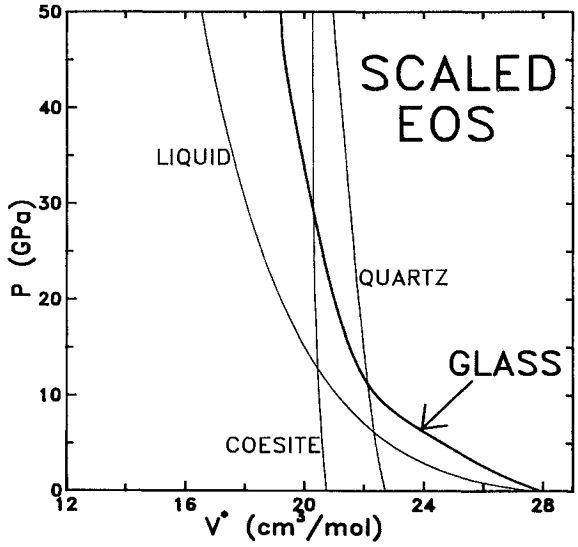

FIG. 10. Scaled equation of state—pressure vs scaled volume $V^* = V[r_{\text{Si-Si}}(0)/r_{\text{Si-Si}}(P)]^3$—for crystalline and amorphous phases of SiO_2. If volume scales with Si-Si distance, V^* is constant and the scaled EOS is a vertical line, which approximates the behavior of the crystals. If Si-Si distance is independent of pressure, the scaled EOS is identical to the standard EOS (P vs V) which approximates the behavior of the liquid. The glass falls in between these two extremes.

its tetrahedral framework, specifically, by increasing the size of its rings, a counterintuitive result which is nevertheless explained by a simple cluster model for the effects of ring formation on density. We now show that this model helps account for the compression of glass as well.

C. Medium-range structure: Clusters

We use a simple cluster model of tectosilicate structures to relate changes in medium-range structure to the compression of the glass.[10] We think of the glass as being composed of only T atoms, each linked to four others through a shared O atom. Each cluster consists of a central T atom, the four T atoms linked to it (the first linked neighbors) all the T atoms linked to these four (the second linked neighbors) and so on. For illustration, in the fourfold-coordinated Bethe lattice, the number of T atoms in the Qth linked neighbor shell, N_Q, and the number of T atoms in a cluster of size Q, M_Q, are given by

$$N_Q = 4 \times 3^{Q-1} , \tag{10}$$

$$M_Q = 1 + \sum_{i=1}^{Q} N_i = 2 \times 3^Q - 1 . \tag{11}$$

For each pressure we have measured mean values of N_Q and M_Q by averaging over all Si atoms in five different configurations, spaced one million configurations apart. In the same way we have also measured D_Q, the average distance from a central atom to atoms in its Qth neighbor shell.

To relate cluster topology (N_Q,M_Q) and geometry (D_Q) to macroscopic density, we assume that the glass structure is composed of clusters of size Q. If we assume that only T atoms in the outermost shell are shared, and that these are shared on average by two clusters, then we can write the macroscopic framework density as

$$\rho_F^* = \frac{\Gamma_Q}{V_Q} , \tag{12}$$

where the star distinguishes the model value from the actual ρ_F, Γ_Q is the cluster population (average number of T atoms in a cluster)

$$\Gamma_Q = M_{Q-1} + \tfrac{1}{2} N_Q \tag{13}$$

and V_Q is the cluster volume

$$V_Q = \frac{4\pi D_Q^3}{3} . \tag{14}$$

The accuracy of the model increases with increasing Q and for $Q=8$ a comparison of ρ_F^* with the actual ρ_F shows that this simple model reproduces macroscopic densities remarkably well (within 6%). More importantly, the compression predicted by (12), that is, the difference in density between compressed and zero pressure volumes, is reproduced very accurately (within 1%). This permits us to separate the compression of the glass into topological (changes in Γ_Q) and geometric (changes in V_Q) components. Defining for simplicity $\Delta X = \ln[X(P)/X(0)]$:

$$\Delta\rho_F^* = \Delta\Gamma_Q - \Delta V_Q . \tag{15}$$

Although ΔV_Q is larger than $\Delta\Gamma_Q$, the topological component of compression is substantial, accounting for 25% of the density increase over the entire pressure range considered here (Fig. 11). Most of the topologic compression is concentrated in a narrow pressure interval between 5 and 10 GPa. This contrasts with the room-temperature behavior of SiO_2 crystals which show no evidence of topologic change below 20 GPa, (Ref. 38). Although, at higher temperatures, crystals undergo topologic compression by way of phase transitions, these are kinetically hindered at 300 K so that quartz, for example, exists up to 22 GPa, tenfold the equilibrium quartz-coesite transition pressure. Thus, topologic change is apparently much more difficult in crystals than in the glass. The presence of undercoordinated "defects"—three coordinated Si atoms and nonbridging O atoms—which are rare in crystals, helps facilitate topologic change in the glass, accounting for its different compressional behavior. Detailed examination of the simulated structures shows that bonding topology is rearranged either by defect healing, in which a nonbridging O atom approaches and finally bonds to a threefold-coordinated Si atom, or by bond switching, in which a bridging O atom approaches and bonds to a threefold-coordinated Si atom, at the same time breaking one of its two original bonds.

On the other hand, the topologic component of compression in the glass is much smaller than in SiO_2 liquid which compresses mostly by topologic change.[11] A comparison of liquid and glass equations of state shows that despite the competing effect of thermal expansion

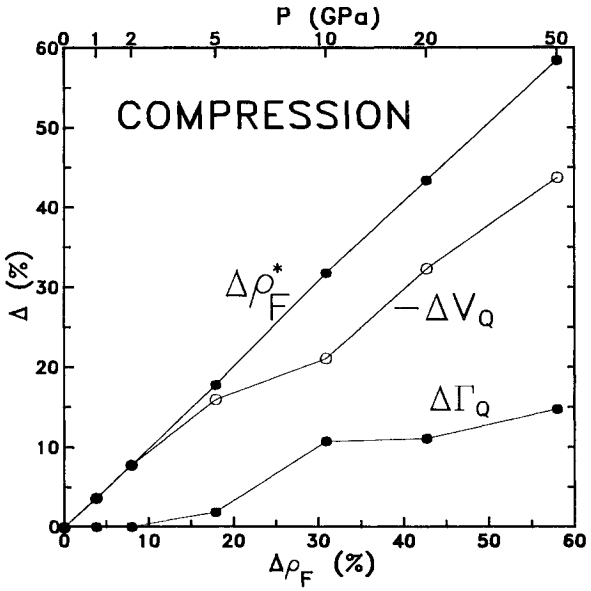

FIG. 11. The change in framework density predicted by the cluster model [$\Delta\rho_F^*$, Eq. (12)] vs the actual change in framework density ($\Delta\rho_F$). The corresponding pressure is indicated on the upper horizontal axis. Also shown are the topological [$\Delta\Gamma_Q$, Eq. (13)] and geometric [ΔV_Q, Eq. (14)] components of the pressure-induced increase in density. Changes in Γ_Q and V_Q are complementary—the pressure interval of greatest topological change coincides with the interval of least geometric change (5–10 GPa). Changes in $r_{\alpha\beta}$ are also unusually small over this pressure interval (Fig. 9).

(the liquid simulations were performed at 2000 K), the liquid is denser than the glass at all pressures (Fig. 2). The more efficient compression of the liquid suggests that kinetic hindrances play an important role in glass compression as well, limiting (but not eliminating) topologic change, and forcing the glass to compress mostly geometrically.

Although the high pressure changes in Γ_Q occur continuously above 5 GPa, the sudden onset of change and the large initial change compared with changes induced by higher pressures are all reminiscent of a pressure-induced phase transition in SiO_2 glass, proposed by Grimsditch[39] on the basis of high pressure Brillouin spectroscopic measurements. A phase transition is a useful, if approximate, picture for glass structure's response to pressure since it evokes reconstruction of the tetrahedral framework. The topologic changes in our simulations are mostly quenchable (preserved on the release of pressure), which accounts for the idea of a phase transition in glass (see also Ref. 40).

D. Medium-range structure: Rings

Measurements of the fundamental ring statistics in our simulated glass, using a new definition of a ring[10] which removes the ambiguities of previous definitions, are shown in Table V. We use these measurements to further elucidate the topological component of compression in the glass with a simple model for the effects of ring formation on framework density. We assume that the relative effects of forming different sized rings is independent of framework type, which allows us to focus on a particularly simple framework, the fourfold coordinated Bethe lattice. Because of the constraint of fourfold coordination, ring formation reduces density by pruning an exactly calculable number of T atoms from the Bethe lattice. The basic result, the relative ability of different sized rings to reduce framework density, is given by the pruning efficiency, $P^*(K)$, the number of T atoms pruned by a K-membered ring in an infinite Bethe lattice, normalized to the number pruned by a three-membered ring:

$$P^*(K)=\begin{cases}\dfrac{1}{3^{1/2(K-1)}} & \text{odd } K\\[2ex] \dfrac{2}{3^{1/2(K-1)}} & \text{even } K\ .\end{cases} \tag{16}$$

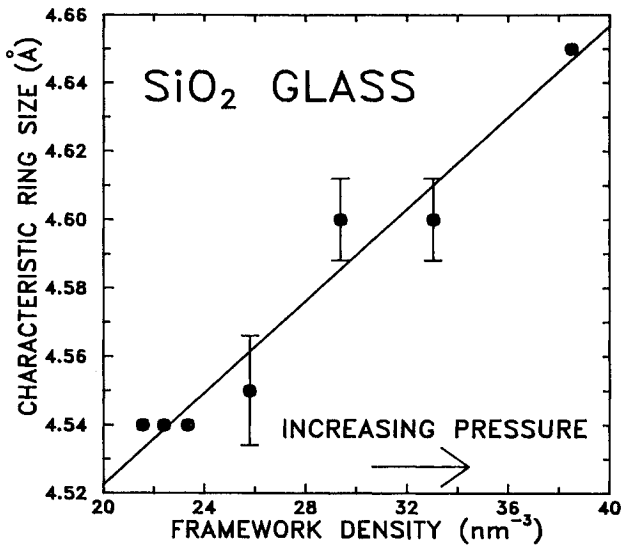

FIG. 12. The characteristic ring size, $K^*(17)$ vs the framework density, ρ_F from the Monte Carlo simulations. The error bars represent the standard deviation in K^* (Table V).

Thus, the model predicts that small rings are exponentially more effective at reducing density than large rings and that some measure of average ring size which takes this into account will increase with increasing density. We define a characteristic ring size, K^*, a weighted average in which $P^*(K)$ is used to take into account the greater importance of small rings:

$$K^*=\frac{\sum_K Kf(K)P^*(K)}{\sum_K f(K)P^*(K)}\ , \tag{17}$$

where $f(K)$ is the average number of K-membered rings passing through a T atom.

We have shown[10,11] that K^* increases upon compression of SiO_2 liquid in our Monte Carlo simulations and with increasing framework density of crystalline tectosilicates, including silica polymorphs, zeolites, and other aluminosilicates. Figure 12 shows that K^* increases with compression of SiO_2 glass as well. The changes in K^* are small compared with those found in the other materials, corresponding to the comparatively small changes in the

TABLE V. Ring statistics. The standard deviation in $f(K)$ among five different configurations is given in parentheses for the last digits reported. If none appears, the quantity is invariant. Rings larger than 12-membered (up to 17-membered rings were found) are not listed since they have a negligible effect on K^* (see text).

		$f(K)$									
P	K^*	$K=3$	$K=4$	$K=5$	$K=6$	$K=7$	$K=8$	$K=9$	$K=10$	$K=11$	$K=12$
0	4.54	0.61	0.69	1.09	0.63	0.55	0.47	0.83	1.13	0.78	2.25
1	4.54	0.61	0.69	1.09	0.63	0.55	0.47	0.83	1.13	0.78	2.25
2	4.54	0.61	0.69	1.09	0.63	0.55	0.47	0.83	1.13	0.78	2.25
5	4.55(2)	0.61	0.69	1.09	0.64(1)	0.57(4)	0.47	0.85(4)	1.09(8)	0.79(2)	2.26(2)
10	4.60(1)	0.61	0.69(5)	1.12(4)	0.68(4)	0.62(5)	0.48	0.96(1)	1.1(2)	0.9(1)	2.4(2)
20	4.60(1)	0.61	0.64(2)	1.17	0.66(4)	0.64(4)	0.48(1)	0.97	1.0(1)	1.03(1)	2.3(1)
50	4.65	0.61	0.69	1.09	0.75	0.77	0.61	0.81	1.20	0.64	3.02

topological component of density (Γ_Q). We attribute the positive correlation of K^* with ρ_F observed in crystalline, liquid, and vitreous states to the greater pruning efficiency of small rings and their consequent tendency to form sparse low-density frameworks. Thus, our theory illustrates the close relation between ring statistics and density for a wide variety of materials and under a wide variety of pressure-temperature conditions, and rationalizes the topological component of compression of SiO_2 glass.

Experimental observation of topological change, specifically the pressure-induced increases in cluster population (13) and characteristic ring size (17) predicted here, remains a significant unsolved challenge. Approximate calculations have suggested a link between Raman spectroscopy and topology.[2] Specifically, the Raman "defect" lines, D_1 and D_2 have been assigned to vibrational modes of four- and three-membered rings, respectively. Thus, the observation that D_2 intensity increases with increasing pressure has been interpreted as an increase in the number of three-membered rings and a decrease in average ring size with compression.[41] This is in sharp contrast to our results which show that if the average ring size changes with compression, it will increase. However, recent, precise calculations of the Raman spectrum of SiO_2 glass suggest that the vibrational mode assignments may be incorrect.[42] These calculations reproduce the observed D_2 line and its increase with pressure, even though the model contains no three-membered rings.

Perhaps the most likely prospect for experimentally confirming our predictions of topological change involves reverse Monte Carlo simulation.[4] This technique, which is similar to Rietveld analysis common in the solution of complex crystal structures, is simply a nonlinear inversion of diffraction data for the (x,y,z) coordinates of Si and O atoms. The result is complete structural information, from which topological parameters such as ring and cluster statistics can be determined. Although the ability of spherically averaged data to uniquely resolve various features of the complete structure would have to be carefully assessed, in principle topological differences between normal and compressed glass could be detected by inverting accurate diffraction data on the two samples. The technique might first be applied to irreversibly compacted samples, for which a diffraction experiment would be free of the limitations of *in situ* high pressure experiments.

VI. CONCLUSIONS

The model accurately predicts nearly all of the structural features of vitreous SiO_2, even though no experimental data on glass were used as constraints. The simulations include the structural elements which are most important for understanding the compression of glass. The predicted combination of medium-range geometrical and topological change leads to excellent agreement with the observed equation of state. The simulations exhibit a rapid, quenchable topological change in medium-range structure between 5 and 10 GPa which supports the idea of a phase transition in glass and readily explains its irreversible compaction. This success, combined with our results for SiO_2 liquid and crystals using the same potential model, indicate that our simulations contain the basic physics of glass compression within the pressure regime of fourfold coordination, to at least 20 GPa.

The simulations predict that the response of SiO_2 glass structure to pressure lies in between two extremes represented by SiO_2 crystals and liquid. While nearest-neighbor interatomic distances shrink with pressure, changes in the network topology of the glass, due to bond breaking and reformation also contribute substantially to compression. Like the compression of SiO_2 liquid, the topological component of compression in the glass is caused by an increase in characteristic ring size, a trend which is mimicked by the positive correlation of ring size and framework density in tectosilicates. We suggest that the most likely prospect for experimental confirmation of the predicted topologic changes involves the analysis of diffraction data with the reverse Monte Carlo technique.

ACKNOWLEDGMENTS

We thank C. Lithgow for helpful comments on the manuscript and R. L. McGreevy for providing the data of Ref. 45. This work was supported by National Science Foundation Grant No. EAR-8816819 and the Institute of Geophysics and Planetary Physics at the Lawrence Livermore National Laboratory. The latter, along with the San Diego Supercomputer Center and the University of California at Berkeley Computing Center, provided generous supercomputer support.

[1] J. C. Phillips, Solid State Phys. **37**, 93 (1982).
[2] F. L. Galeener, Solid State Commun. **44**, 1037 (1982).
[3] D. J. Grimley, A. C. Wright, and R. N. Sinclair, J. Non-Cryst. Solids **119**, 49 (1990).
[4] D. A. Keen and R. L. McGreevy, Nature (London) **344**, 423 (1990).
[5] W. H. Zachariasen, J. Am. Chem. Soc. **54**, 3841 (1932).
[6] F. L. Galeener, in *The Physics and Technology of Amorphous SiO_2*, edited by R. A. B. Devine (Plenum, New York, 1988), p. 1.
[7] R. J. Bell and P. Dean, Nature (London) **212**, 1355 (1966).
[8] L. F. Gladden, J. Non-Cryst. Solids **119**, 318 (1990).
[9] F. Wooten and D. Wearie, Solid State Phys. **40**, 1 (1987).
[10] L. Stixrude and M. S. T. Bukowinski, Am. Mineral. **75**, 1159 (1990).
[11] L. Stixrude and M. S. T. Bukowinski, Science **250**, 541 (1990a).
[12] L. Stixrude and M. S. T. Bukowinski, Phys. Chem. Minerals **16**, 199 (1988).
[13] L. Stixrude and M. S. T. Bukowinski, Geophys. Res. Lett. **16**,

1403 (1989).
[14]Q. Williams, R. Jeanloz, Science **239**, 902 (1988).
[15]L. V. Woodcock, C. A. Angell, and P. Cheeseman, J. Chem. Phys. **65**, 1565 (1976).
[16]J. D. Kubicki and A. C. Lasaga, Am. Mineral. **73**, 941 (1988).
[17]S. Tsuneyuki, M. Tsukada, H. Aoki, and Y. Matsui, Phys. Rev. Lett. **61**, 869 (1988).
[18]J. R. Rustad, D. A. Yuen, and F. J. Spera, Phys. Earth Planet. Int. **65**, 210 (1991).
[19]R. L. Erikson and C. J. Hostetler, Geochim. Cosmochim. Acta **51**, 1209 (1987).
[20]M. A. Spackman, R. J. Hill, and G. V. Gibbs, Phys. Chem. Minerals **14**, 139 (1987).
[21]J. P. Hansen and I. R. McDonald, *Theory of Simple Liquids* (Academic, New York, 1986).
[22]The de Broglie thermal wavelength is $\Lambda=(h^2/2\pi mkT)^{1/2}=0.007$ Å, where h is Planck's constant, k is Boltzmann's constant, T is 300 K, and m, the mean atomic weight, is 20 amu, and the average interatomic separation is $a=(V/N)^{1/3}=2.5$ Å, where V/N is the average volume per atom.
[23]H. Flyvbjerg and H. G. Petersen, J. Chem. Phys. **91**, 461 (1989).
[24]B. D. Ripley, *Stochastic Simulation* (Wiley, New York, 1987).
[25]C. Meade and R. Jeanloz, Phys. Rev. B **35**, 236 (1987).
[26]P. W. Bridgman, Proc. Am. Acad. Arts Sci. **76**, 55 (1948).
[27]S. P. Marsh, *LASL Shock Hugoniot Data* (University of California, Berkeley, 1990).
[28]Y. Tsuchida and T. Yagi, Nature (London) **340**, 217 (1989).
[29]G. E. Bacon, Acta Crystallogr. A **25**, 391 (1969).
[30]D. T. Cromer and J. T. Waber, Acta Crystallogr. **18**, 104 (1965).
[31]P. Vashishta, R. K. Kalia, J. P. Rino, and I. Ebbsjö, Phys. Rev. B **41**, 12197 (1990).
[32]L. Guttman and S. M. Rahman, Phys. Rev. B **37**, 2657 (1988).
[33]B. P. Feuston and S. H. Garofalini, J. Chem. Phys. **89**, 5818 (1988).
[34]J. L. Robertson and S. C. Moss, J. Non-Cryst. Solids **106**, 330 (1988).
[35]R. L. Mozzi and B. E. Warren, J. Appl. Crystallogr. **2**, 164 (1969).
[36]R. F. Pettifer, R. Dupree, I. Farnan, and U. Stenberg, J. Non-Cryst. Solids **106**, 408 (1988).
[37]R. Couty, Thèse de Doctorat d'Etat, Université de Paris VI, 1977; P. McMillan, B. Piriou, and R. Couty, J. Chem. Phys. **81**, 4234 (1984).
[38]R. J. Hemley, A. P. Jephcoat, H. K. Mao, L. C. Ming, and M. H. Manghnani, Nature (London) **334**, 52 (1988).
[39]M. Grimsditch, Phys. Rev. Lett. **52**, 2379 (1984).
[40]L. Stixrude and M. S. T. Bukowinski, EOS, Trans. Am. Geophys. Union **71**, 1671 (1990); L. Stixrude and M. S. T. Bukowinski (unpublished).
[41]R. J. Hemley, H. K. Mao, P. M. Bell, and B. O. Mysen, Phys. Rev. Lett. **57**, 747 (1986).
[42]R. A. Murray and W. Y. Ching, Phys. Rev. B **39**, 1320 (1989).
[43]J. H. Konnert and J. Karle, Acta Crystallogr. A **29**, 702 (1973).
[44]Y. Waseda and H. Suito, Trans. Iron Steel Inst. Jpn. **17**, 82 (1977).
[45]J. B. van Tricht (unpublished).